Accepted Manuscript

Research papers

Evaluation of the Gridded CRU TS Precipitation Dataset with the Point Raingauge Records over the Three-River Headwaters Region

Haiyun Shi, Tiejian Li, Jiahua Wei

PII: S0022-1694(17)30154-3
DOI: http://dx.doi.org/10.1016/j.jhydrol.2017.03.017
Reference: HYDROL 21874

To appear in: *Journal of Hydrology*

Received Date: 9 January 2017
Revised Date: 9 February 2017
Accepted Date: 8 March 2017

Please cite this article as: Shi, H., Li, T., Wei, J., Evaluation of the Gridded CRU TS Precipitation Dataset with the Point Raingauge Records over the Three-River Headwaters Region, *Journal of Hydrology* (2017), doi: http://dx.doi.org/10.1016/j.jhydrol.2017.03.017

Evaluation of the Gridded CRU TS Precipitation Dataset with the Point Raingauge Records over the Three-River Headwaters Region

Haiyun SHI [a,b,c,d,*], Tiejian LI [a,b,c], Jiahua WEI [a,b,c]

[a] *State Key Laboratory of Plateau Ecology and Agriculture, Qinghai University, Xining, Qinghai, China*

[b] *School of Water Resources and Electric Power, Qinghai University, Xining, Qinghai, China*

[c] *State Key Laboratory of Hydroscience and Engineering, Tsinghua University, Beijing, China*

[d] *Department of Civil Engineering, The University of Hong Kong, Hong Kong, China*

Haiyun SHI: shihaiyun@tsinghua.edu.cn

Tiejian LI: litiejian@tsinghua.edu.cn

Jiahua WEI: weijiahua@tsinghua.edu.cn

*Corresponding author (Dr. Haiyun SHI).

Revised manuscript for the *Journal of Hydrology*

February 2017

Abstract

This study evaluated the performance of the gridded CRU TS precipitation dataset in describing the spatial and temporal characteristics of precipitation over the Three-River Headwaters Region (TRHR) during 1961-2014, and the results were compared with those derived from the point raingauge records (RGR) at 29 meteorological stations. It indicated that: (1) temporally, the TRHR has experienced a significant increasing trend in the annual precipitation during 1961-2014; (2) spatially, the mean annual precipitation (MAP) in the TRHR showed the southeast-to-northwest decreasing trend; (3) a close correlation of the MAP with elevation was found, and statistical equations to estimate the MAP derived from the gridded CRU TS dataset were established based on longitude, latitude and elevation. Through comparing the results derived from these two datasets, it is concluded that the CRU TS dataset gave a lower estimation of annual precipitation than that from the RGR data but similar variation characteristics. Moreover, the MAP values derived from the gridded CRU TS dataset could be well estimated by the equations derived from the RGR data. The results would be valuable for the researchers to make better use of this gridded precipitation dataset and have a clearer understanding of the spatio-temporal patterns of precipitation in similar high-elevation mountainous regions such as the TRHR, where ground precipitation measurements are not widely available.

Keywords: Precipitation; Gridded CRU TS dataset; Point raingauge records; Three-River Headwaters Region

1. Introduction

Precipitation is regarded as one of the basic components in the global energy and water cycles and has been widely used in the fields of integrated water resources management, crop water requirements prediction, and ecological environment assessment. In the past several decades, global climate change has greatly affected the water circulation and hydrological processes, which indeed caused dramatic changes in precipitation in most regions (Liu et al., 2008; IPCC, 2013; Chen and Chu, 2014; Shi and Wang, 2015; Zarch et al., 2015), and therefore, high-accuracy precipitation data seem to be necessary for studies on meteorology, hydrology, water resources and climate change. Normally, precipitation can be estimated from a variety of sources, such as the point raingauge records (noted as RGR hereafter) and the gridded datasets by interpolation and assimilation from station and/or satellite data (Dirks et al., 1998; Kistler et al., 2001; Nezlin and Stein, 2005; Mishra et al., 2011; Harris et al., 2014). Although the RGR is regarded to be relatively accurate and reliable at the point where a raingauge station locates, the density of the raingauge network is usually not high enough to accurately describe the spatial distribution and changes of precipitation. Hence, the widely-applied gridded datasets, which can provide important information about the areal estimates, are regarded to be a viable supplement for the RGR (Bosilovich et al., 2008; Li et al., 2012; Woldemeskel et al., 2013; Schneider et al., 2014). However, the inevitable errors of the precipitation estimated by the gridded datasets cannot be totally ignored because they may not be as accurate as the RGR for a designated point and include considerable uncertainties. Generally, the gridded datasets should be verified before they are applied in the water-related issues (e.g., flood forecast, drought assessment and natural ecosystem evaluation) for the designated regions (Silva et al., 2011; Sohn et al., 2012; Shi, 2013; Lin et al., 2014; Zhu et al., 2015; Jones et al., 2016).

Currently, the global gridded precipitation datasets have been developed by a number of research institutes, such as the Climatic Research Unit (CRU) at the University of East Anglia, the Global Precipitation Climatology Centre (GPCC) at Deutscher Wetterdienst and the National Oceanic and Atmospheric Administration (NOAA) (Becker et al., 2013; Schneider et al., 2014; Harris and Jones, 2015). Evaluations of these datasets have also been conducted all around the world, e.g., in China (Zhao and Fu, 2006; Ma et al., 2009; Zhu et al., 2015; Chen et al., 2016), Iberian Peninsula (Belo-Pereira et al., 2011), Iran (Khalili and Rahimi, 2014), and Caribbean (Jones et al., 2016), indicating the overall good performances of these datasets in researches on hydro-meteorological forecast and climate change in spite of certain limitations (e.g., errors). It is worth noting that, according to some of the studies focused on China (Zhao and Fu, 2006; Ma et al., 2009), better performances have been found in eastern China rather than western China for most datasets. The reason for this is that topography is totally different in eastern China (i.e., mainly plains and hills) and western China (i.e., mainly plateaus and mountains), leading to the uneven distribution of meteorological stations in eastern China and western China. Specifically, for the Tibet Plateau region, Chen et al. (2016) pointed out that the reanalysis data from the National Center for Atmospheric Research (NCAR) would reveal strong anisotropy in spatial coherence of climate variations.

The Three-River Headwaters Region (noted as TRHR hereafter), which is well-known as the sources of the Yangtze River, the Yellow River and the Lantsang River, is located in the Qinghai Province in western China. With an area of 0.3 million km^2, it accounts for

43% of the total area of the Qinghai Province (Cao and Pan, 2014). As a plateau region, the elevation varies between 2,000 m and 6,600 m, and the mean value is over 4,000 m. Moreover, this region lies in the temperate zone, and the annual precipitation ranges from 262 mm to 773 mm (Yi et al., 2013), over 80% of which occurs in the wet season from May to October (Liang et al., 2013; Shi et al., 2016a). The TRHR is particularly sensitive to climate change, which may bring serious disturbances to the ecosystem (Fan et al., 2010; Immerzeel et al., 2010; Zhang et al., 2013; Tong et al., 2014). For example, several studies (Liang et al., 2013; Yi et al., 2013; Shi et al., 2016a) have reported an increasing trend in the annual precipitation over the TRHR during the past several decades. Tong et al. (2014) indicated that the annual precipitation generally showed an increasing trend from 1990 to 2012, and such trend was more obvious with significant fluctuations after 2004. However, the results in these previous studies were all obtained from the analyses of the RGR data; the application of the gridded precipitation datasets in this region cannot be found in the literature. Thus, it is important and necessary to evaluate the performances of the gridded precipitation datasets in describing the spatial and temporal characteristics of precipitation over the TRHR.

To this end, this study aims to evaluate the gridded precipitation dataset with the point RGR data over the TRHR. First, the spatio-temporal patterns of precipitation over this region will be investigated using the gridded precipitation dataset and the point RGR data, respectively. Second, the relationship of precipitation derived from the gridded dataset with elevation will be analyzed. Third, with a comprehensive comparison conducted based on the obtained results, the reliability of the gridded precipitation dataset will be discussed. Since the gridded dataset and the point RGR data have their own levels of uncertainties, the results of this study will provide the more realistic and reliable analyses of the spatio-temporal patterns of precipitation. For the similar high-elevation mountainous regions such as the TRHR, where ground precipitation measurements are not widely available, it is believed that other types of precipitation data (including the gridded dataset) will be more important, and this study will be helpful to provide a scientific basis for making better use of the gridded precipitation dataset. The remainder of this paper is organized as follows. Section 2 gives a brief introduction of the research data. Section 3 shows the main methodologies used in this study. The results and discussion follow in Section 4 and the final section displays the conclusions of this study.

2. Research data

This study employs two sources of precipitation data, including the gridded dataset and the point RGR data. The Climatic Research Unit Time-Series (noted as CRU TS hereafter) Version 3.23 dataset is selected as the representative of the gridded datasets, which can provide the month-by-month variations in climate over the period 1901-2014, on high-resolution (i.e., 0.5×0.5 degree) grids (Harris and Jones, 2015). Moreover, the RGR data of 37 meteorological stations available inside or around the TRHR are downloaded for free from the official website of China Meteorological Administration (China Meteorological Administration, 2016), which are at the daily time scale.

2.1. The RGR data

There are 37 meteorological stations available inside or around the TRHR (Fig. 1 and Table 1). As most of these stations were built in the late 1950s, only the data from 1961 are selected in this study to ensure that the lengths of the series from different stations are consistent. For the designated station, missing data in a certain year are interpolated using the data of the neighboring stations in the same year; however, stations with lack of data for more than twenty years are excluded directly (the blue points in Fig. 1 and the stations in italic format in Table 1). After this elimination, there are 29 meteorological stations left with complete daily observations from 1961 to 2014, among which, 17 stations are located inside the TRHR (the green points in Fig. 1 and the stations in bold format in Table 1) and the others outside. For each station, the annual precipitation can be derived from the daily values, and in order to obtain the annual precipitation over the TRHR for each year, the inverse distance weighting (noted as IDW hereafter) method (see subsection 3.2 for details) is adopted to interpolate the annual precipitation from different stations. Moreover, the yearly anomalies can be achieved by removing the long-term mean annual precipitation (noted as MAP hereafter).

2.2. CRU TS Version 3.23

This dataset is produced by the CRU in University of East Anglia, England, including a number of variables (e.g., cloud cover, precipitation, temperature, vapor pressure, potential evapotranspiration, and frost day frequency) at the monthly time scale from January 1901 to December 2014. This dataset is derived from the daily or sub-daily observational data by National Meteorological Services and other agents. In general, station anomalies are spatially interpolated into 0.5×0.5 degree grids covering the global land surface excluding Antarctica, and combined with an existing climatology to obtain absolute monthly values. More details about data interpolation and quality assessment can be found in the studies of Harris et al. (2014) and Harris and Jones (2015). Compared to the earlier versions, this dataset added some new stations for precipitation and temperature and updated the series with 2014 data; however, the same methodology as for the earlier version (i.e., *Version 3.21*) was used.

Within the range of the TRHR, there are totally 153 CRU TS grids with horizontal resolution of 0.5×0.5 degree. Fig. 1 shows the distribution of these grids, and only the central point of each grid is presented in this figure. For each grid, the annual precipitation can be easily calculated as the sum of the monthly values, and the annual precipitation over the TRHR for each year can be obtained by averaging the annual precipitation of all the grids. Moreover, the yearly anomalies can be achieved by removing the long-term MAP. It is worth noting that only the data during the period 1961-2014 are used in this study according to the series length of the RGR data.

3. Methodology

3.1. Trend test and change point test methods

A number of previous studies have proved that the Mann-Kendall trend test and the Pettitt change point test methods are useful for researches on meteorology, hydrology and sedimentology (e.g., Mu et al., 2007; Jones et al., 2015; Shi and Wang, 2015; Zhang et al., 2015; Shi et al., 2016a, 2016b; Shi et al., 2017). The Mann-Kendall trend test is a non-parametric rank-based statistical test that was first proposed by Mann (1945) and further developed by Kendall (1975). Then, the slope of the series can be computed using the Thiel-Sen method (Thiel, 1950; Sen, 1968). Moreover, prewhitening (von Storch and Navarra, 1995) is required to eliminate the influence of autocorrelation because such series is not applicable for the Mann-Kendall trend test method. The Pettitt change point test is a non-parametric rank-based statistical test used to identify the change points in the series

(Pettitt, 1979). When the first change point is found, the series will be divided into two subsequences; and additional change points in these subsequences may generate more subsequences.

3.2. Spatial interpolation method

In order to compute the spatial distribution of precipitation described by the point RGR data over the TRHR, a spatial interpolation method is necessary. Considering both the simplicity and the accuracy of interpolating meteorological variables, this study selects the IDW method (Shi et al., 2014). As a widely-used geometric method, the general form of this method can be expressed as follows:

$$P_p = \frac{\sum_{i=1}^{N} \frac{1}{D_i^{\beta}} P_i}{\sum_{i=1}^{N} \frac{1}{D_i^{\beta}}} \qquad (1)$$

where N is the number of used meteorological stations, P_p is the interpolated value at the place of interest, P_i is the value at the i-th given station, D_i is the distance from the i-th given station to the place of interest, and β is the power of D_i. Following common practice (e.g., Goovaerts, 2000; Mito et al., 2011; Shi et al., 2016a, 2017), this study adopted the value β to be 2, and the IDW method turns into the so-called inverse distance squared method.

To match the horizontal resolution of the CRU TS dataset, the places of interest over the whole study area are defined as continuous grids with a size of 0.5 degree. For each year, the annual precipitation from different stations can be interpolated using the IDW method to get the annual precipitation at any place of interest, with which we can obtain the spatial distribution of annual precipitation over the TRHR.

3.3. Normalization method

In order to facilitate the evaluation of the gridded CRU TS precipitation dataset with the point RGR over the TRHR, it is better to use the normalized values rather than the original values for comparison. Generally, the normalization method is as follows:

$$NX_i = \frac{X_i - X_{\min}}{X_{\max} - X_{\min}} \tag{2}$$

where NX_i is the normalized value, X_i is the i-th original value, and X_{max} and X_{min} are the maximum and minimum values among all the original values, respectively.

3.4. Assessment criteria

In order to quantify the errors of the gridded CRU TS precipitation dataset, two objective functions are used as assessment criteria, namely, Relative Error (RE) and Nash-Sutcliffe Coefficient of Efficiency (NSCE) (Nash and Sutcliffe, 1970). The equations of RE and NSCE are given as follows:

$$RE = (X_{i,grid} - X_{i,RGR}) / X_{i,RGR} \tag{3}$$

$$NSCE = 1 - \frac{\sum_{i=1}^{N}\left(X_{i,grid} - X_{i,RGR}\right)^2}{\sum_{i=1}^{N}\left(X_{i,RGR} - \overline{X_{RGR}}\right)^2} \tag{4}$$

where $X_{i,grid}$ and $X_{i,RGR}$ are the i-th values derived from the gridded dataset and the RGR data, respectively; $\overline{X_{RGR}}$ is the mean value of the RGR data; and N is the sample size.

4. Results and discussion

4.1. The gridded CRU TS precipitation dataset

4.1.1 Spatial-temporal characteristics of precipitation

Based on the annual precipitation series (1961-2014) derived from the gridded CRU TS dataset, the trend test and change point test were conducted to investigate the temporal characteristics of the annual precipitation over the TRHR. The black dash line in Fig. 2 shows the variation of the annual precipitation presented by the CRU TS dataset. It is observed that the MAP over the TRHR was 224.0 mm during 1961-2014, and the annual precipitation series showed a significant increasing trend with the change rate of 8.08 mm/decade (p<0.1). Moreover, the result of change point test showed that the change point was found in 1997 at the significance level of 0.1 (Table 2). However, no additional change points were found in the two subsequences; and therefore, the annual precipitation series was divided into two parts, namely, 1961-1997 and 1998-2014, respectively. The two grey dash lines showed the MAP of the two subsequences (Fig. 2). The MAP was 213.7 mm during 1961-1997, which was a little smaller than the long-term mean value (i.e., 224.0 mm); moreover, a non-significant increasing trend with the change rate of 0.39 mm/decade was found in this period (p>0.1). By contrast, the MAP reached 246.5 mm during 1998-2014, which was much larger than the long-term mean value (i.e., 224.0 mm); moreover, a non-significant increasing trend with the change rate of 2.53 mm/decade was found in this period (p>0.1).

With reference to the spatial characteristics of the annual precipitation over the TRHR during 1961-2014, the MAP in each grid was calculated through averaging the annual precipitation of each year. Fig. 3 shows the spatial distribution of the MAP in each grid over the TRHR during 1961-2014. Generally, the MAP showed the southeast-to-northwest decreasing trend over this region, with the highest value of 404.4 mm at the southeastern edge of this region and the lowest value of only 88.1 mm at the northwestern edge. The highest value was more than four times larger than the lowest one. The reason for this is as follows: the TRHR lies in a typical plateau continental monsoon region where precipitation is mainly dominated by the South Asian Monsoon (noted as SAM hereafter) (Yu et al., 2009; Boos and Kuang, 2010; Cao and Pan, 2014); moreover, it is located in the north of the Tibetan Plateau, the mountainous topography of which may play an important role in blocking a proportion of the moisture delivered by the SAM from the Indian Ocean. As a result, for a designated location in the TRHR, there will be less precipitation if it is farther from the Indian Ocean, leading to the south-to-north decreasing trend over this region. In addition, Liang et al. (2013) reported that the climate in the TRHR can also be influenced by the East Asian Monsoon, which may cause the east-to-west decreasing trend over this region. Moreover, the spatial distribution of the change rate of the annual precipitation in each grid over the TRHR during 1961-2014 was shown in Fig. 4. It is clear that the annual precipitation of all the 153 grids presented the increasing trends, with the highest change rate (14.6 mm/decade, $p<0.01$) in the central part (near the Maduo station) and the lowest change rate (2.37 mm/decade, $p<0.05$) at the northwestern edge (near the Wudaoliang station). It is worth noting that only the trends of 6 grids were statistically non-significant ($p>0.1$), and three of them were located in the east part of the TRHR and the other three were located in the west part (Fig. 4), which can be explained by different reasons. The non-significant trends of the 3 grids in the east part were caused by the relatively higher

MAP (i.e., 404.3, 385.6 and 363.6 mm, ranking the 1^{st}, 4^{th} and 10^{th} highest of all the 153 grids, respectively) and relatively lower change rate (i.e., 4.82, 5.33 and 4.61 mm/decade, ranking the 24^{th}, 32^{nd}, and 22^{nd} lowest of all the 153 grids, respectively), while the non-significant trends of the other 3 grids were mainly due to the quite low change rate (i.e., 2.79, 2.88 and 3.32 mm/decade, ranking the 4^{th}, 5^{th} and 10^{th} lowest of all the 153 grids, respectively) and relatively higher MAP (i.e., 163.7, 118.6 and 140.4 mm) than those of the rest of the top ten (i.e., the highest MAP of the other 7 grids was only 103.4 mm).

4.1.2 Relationship between precipitation and elevation

The changing characteristics of precipitation along with elevation change have been reported by previous studies (Schermerhorn, 1967; Goovaerts, 2000; Chu, 2012; Shi, 2013; Shi et al., 2016a). In order to analyze the relationship between precipitation derived from the gridded CRU TS dataset and elevation over the TRHR, the Advanced Spaceborne Thermal Emission and Reflection Radiometer (ASTER) Global DEM dataset (ASTER GDEM Validation Team, 2009, 2011) was used in this study. The original grids with the horizontal resolution of 30×30 m were aggregated to grids with a size of 0.5 degree, which could match the horizontal resolution of the CRU TS dataset and be used to compute the average elevation of each grid.

Fig. 5 shows the relationship between the MAP and elevation in each grid over the TRHR during 1961-2014. It is clear that the 153 grids could be divided into two groups, and the cutoff value should be 3,800 m in this region according to our previous study (Shi et al., 2016a). Group I included 22 grids with the elevations lower than 3,800 m, mainly located in the northeastern part of the TRHR; while the other 131 grids with the elevations higher than 3,800 m were regarded as Group II. In order to obtain the more significant trends for these two groups, some grids with the elevations lower than 3,000 m or higher than 5,000 m (i.e., the hollow circles in Fig. 5) were considered as outliers in this study. For the grids with elevations lower than 3,000 m (2 in total), local climate may be influenced by human activities more easily; while for the grids with elevations higher than 5,000 m (18 in total), the dominant factors which can influence local climate may be quite different (Curio and Scherer, 2016; Huang et al., 2016). As a result, there were 20 grids left in Group I and 113 grids left in Group II, respectively. The MAP values of the selected grids in Group I increased along with elevation increase, and the change rate was 185 mm/km (R^2 = 0.42). In contrast, for the selected grids in Group II, an inverse correlation was found between the MAP and elevation (i.e., -187 mm/km, R^2 = 0.36). In addition, the geographical location (i.e., longitude and latitude) is regarded as an important factor in influencing precipitation, and therefore, the longitude and latitude of the selected grids were also taken into account to establish better relationship between precipitation and elevation. The statistical equations to estimate the MAP derived from the gridded CRU TS dataset were expressed as follows, which were obtained by using the multiple regression method.

$$P = \begin{cases} 33.26X - 49.39Y - 0.008Z - 1306, & Z < 3800m, \quad R^2 = 0.99 \\ 16.14X - 38.24Y - 0.017Z + 56, & Z \geq 3800m, \quad R^2 = 0.84 \end{cases} \tag{5}$$

where P denotes the MAP (mm), X and Y denote the longitude and latitude of each grid, and Z denotes the elevation of each grid (m). The R^2 values were quite high, which were 0.99 for Group I and 0.84 for Group II, respectively. Equation (5) indicated that the MAP derived from the gridded CRU TS dataset during 1961-2014 presented the east-to-west and south-to-north decreasing trends over the TRHR, which were consistent with the analyses in subsection 4.1.1 (Fig. 3). However, it is worth noting that the coefficient of *Z* for Group I was a negative number, which was inconsistent with the previous analyses. The reason for this is as follows: elevation information can be implied in the geographical location (i.e., longitude and latitude) to some extent; and therefore, the coefficients of *X* and *Y* may partly represent the impact of elevation on the MAP over the TRHR, accordingly affecting the coefficient of *Z*.

Fig. 6 shows the comparison of the MAP values estimated by equation (5) and the observations in each grid of the CRU TS dataset. It is worth noting that the results of the grids in Group I were much better than those in Group II. All the RE values of the grids in Group I were within ±20%, and the largest RE value was only -3.2%. In contrast, there were 101 grids (113 in total) in Group II having the RE values within ±20%, and the largest RE value reached -56.3%. Moreover, the large RE values mainly appeared in the grids with high elevations, i.e., larger than 4,700 m. The RE values of the outliers (i.e., 2 grids with elevations lower than 3,000 m and 18 grids with elevations higher than 5,000 m) were also computed using equation (5) although they were not used for regression, and the results were shown in Fig. 6 (i.e., the hollow circles). The RE values of 12 grids (20 in total) were within ±20%, and the largest RE value was -45.8%, which indicated the overall good performance of equation (5) in estimating the MAP values of the outliers.

4.2. The RGR data

In our previous study (Shi et al., 2016a), the annual precipitation series (1961-2014) derived from the RGR data have been used to investigate the changing characteristics of precipitation over the TRHR. However, in order to obtain the annual precipitation over the TRHR for each year, the Thiessen polygon method (Thiessen and Alter, 1911; Brassel and Reif, 1979) was adopted in our previous study to interpolate the annual precipitation from different stations. In contrast, this study employs the IDW method, which can present smoother and more accurate interpolation results than the Thiessen polygon method (Goovaerts, 2000; Shi et al., 2014). Thus, there are a few differences between the results of this study and our previous study.

The black solid line in Fig. 2 shows the variation of the annual precipitation presented by the RGR data at the 29 meteorological stations. As shown in Table 2, the MAP was 406.0 mm over the TRHR during 1961-2014, which was a little smaller than that in our previous study (i.e., 423.0 mm) but much larger than that derived from the gridded CRU TS dataset (i.e., 224.0 mm). The annual precipitation series showed a significant increasing trend with the change rate of 6.82 mm/decade (p<0.1), and only one change point was found in 2002 at the significance level of 0.1. As a result, the annual precipitation series was divided into two parts (i.e., 1961-2002 and 2003-2014). The two grey solid lines in Fig. 2 showed the MAP of the two subsequences. The MAP during 1961-2002 was 397.0 mm, showing a decreasing trend with the change rate of -2.45 mm/decade, while the MAP during 2003-2014 was 437.5 mm, showing a significant increasing trend with the change rate of 18.6 mm/decade.

Furthermore, the MAP in each station located inside the TRHR was calculated through averaging the annual precipitation of each year during 1961-2014 (Fig. 3). It is observed that the Jiuzhi station, which locates at the southeastern edge of this region, had the highest MAP of 745.9 mm; while the stations with the lower MAP were located in the northern part of this region, namely, the Tuotuohe station (294.8 mm) and the Wudaoliang station (291.9 mm) in the northwest, and the Guizhou station (255.6 mm) in the northeast. However, the MAP over the TRHR also showed the overall southeast-to-northwest decreasing trend, the same as that presented by the gridded CRU TS dataset. The spatial distribution of the change rates of the annual precipitation in the 17 stations located inside the TRHR during 1961-2014 was also shown in Fig. 4. The annual precipitation in 15 stations presented the increasing trends, and the trends in 9 stations of them were statistically significant (p<0.1). Among them, the Wudaoliang station had the highest change rate (19.0 mm/decade, p<0.01), followed by the Qumalai station (15.63 mm/decade, p<0.01) and the Maduo station (15.57 mm/decade, p<0.01). However, the annual precipitation of the remaining 2 stations presented the decreasing trends, among which, only the trend in the Henan station was statistically significant (-11.06 mm/decade, p<0.1).

4.3. Comparison of the results derived from the two datasets

4.3.1 Annual precipitation series

As shown in Fig. 2 and Table 2, the annual precipitation values derived from the CRU TS dataset were much smaller than those derived from the RGR data, although the same trends were found in these two annual precipitation series. Table 3 lists the results of the RE analysis for the annual precipitation series derived from these two datasets over the TRHR during 1961-2014. Generally, the RE values varied from -50% (in 1999) to -36% (in 2007) except the year 2002, which had the smallest RE value of only -9%, and the mean RE value was -45% during 1961-2014 (except 2002). Fig. 7 shows the relationship between the annual precipitation series derived from these two datasets over the TRHR during 1961-2014, in which the point represented the year 2002 was far away from those represented other years. Excluding this point, the relationship could approximately be expressed using the linear regression method as follows:

$$P_{CRU\ TS} = 0.55 P_{RGR} \tag{6}$$

where $P_{CRU\ TS}$ denotes the annual precipitation derived from the gridded CRU TS dataset (mm) and P_{RGR} denotes the annual precipitation derived from the point RGR data (mm). The high R^2 value (0.77) indicated the good performance of this linear regression equation.

Nevertheless, the variations of the annual precipitation series derived from the CRU TS dataset and the RGR data were greatly similar. Fig. 8a shows the anomalies of the annual precipitation series derived from these two datasets over the TRHR during 1961-2014, which indicated that the dash line could basically overlap the solid line except 2002. To facilitate the evaluation of the performance of the gridded CRU TS precipitation dataset, the normalized anomalies of the annual precipitation series derived from these two datasets were computed for comparison, and Fig. 8b shows the relevant result. The scattered points were almost distributed near the 45° line, and the NSCE value was 0.76. It indicated that the normalized anomalies of the gridded CRU TS dataset could well match those of the RGR data, and the annual precipitation derived from these two datasets had the similar variation characteristics during 1961-2014.

Moreover, for either of these two datasets, the MAP value during the period after the change point was much larger than before (Table 2), i.e., with the increment of 32.8 mm for the gridded CRU TS dataset and 40.5 mm for the RGR data, respectively. In addition to the significant influence of climate change in recent decades (e.g., global warming), the other reasons for this may be as follows: first, the policies of the Grain to Green Program and Natural Forest Conservation Program in China started from 1999, and were fully implemented from 2002. In particular for the TRHR, the Ecological Protection and Reconstruction Program which started from 2005 has significantly changed the underlying surface conditions and affect the water circulation and hydrological processes in this region (Shi et al., 2016b). Shao et al. (2010) showed that the land cover condition in the TRHR was experiencing the ameliorative stage from 2004 to present. Second, the policy of the Artificial Precipitation Program in the TRHR began from 2005, almost covering the whole TRHR. Therefore, the MAP values during the period 2005-2014 were even larger, namely, 248.0 mm the gridded CRU TS dataset and 439.8 mm for the RGR data, respectively.

4.3.2 The MAP and change rate in each station and the corresponding grid

From Figs. 3 and 4, it is clear that the location of each station for the RGR data can correspond to a grid for the CRU TS dataset. Therefore, the MAP and change rate in each station (i.e., the values out of parentheses) and the corresponding grid (i.e., the values in parentheses) can be obtained, and the comparison results are listed in Table 4. Generally, the RE values of the MAP varied from -64% (in the Wudaoliang station) to -18% (in the Qiaboqia station) except the Guizhou station, which had the positive RE value of 10%. The mean RE value was -40% for all the 17 stations, and if excluding the RE value of the Guizhou station, the mean RE value for the remaining 16 stations would be -43%, which was close to the mean RE value of the annual precipitation series (i.e., -45%) obtained in subsection 4.3.1. Moreover, the relationship between the RE values of the MAP and elevation for each station located inside the TRHR and the corresponding grid was investigated (Fig. 9). The RE values would be larger along with elevation increase, and the

R^2 value for this linear regression was high (i.e., 0.71). In contrast, the RE values of the change rate seemed to be much larger, which varied from -196% (in the Jiuzhi station) to 246% (in the Yushu station). The results indicated the significant differences between the change rates derived from the CRU TS dataset and the RGR data.

Furthermore, based on the statistical equations to estimate the MAP derived from the RGR data proposed by Shi et al. (2016a) and equation (6) in this study, the MAP in each grid corresponding to the station located inside the TRHR could be estimated as follows:

$$P_{CRU\_TS} = \begin{cases} 24.43X - 33.85Y + 0.106Z - 1362, & Z < 3800m \\ 10.88X - 48.82Y - 0.014Z + 910, & Z \geq 3800m \end{cases} \tag{7}$$

Table 5 lists the comparison of the MAP values estimated by equations (5) and (7) for each grid corresponding to the station located inside the TRHR. It is observed that the results obtained from equation (5) were generally better than those obtained from equation (7). By using equation (5), the RE values of 16 grids (except the grid corresponding to the Wudaoliang station) were within ±20%, and the largest RE value was 25.1%; while there were only 14 stations having the RE values within ±20% by using equation (7), and the largest RE value was -39.9%. However, the largest RE value by using equation (7) was not quite large, which indicated that the MAP values derived from the gridded CRU TS dataset could be well estimated by using equation (7) which was derived from the RGR data.

5. Conclusions

This study evaluated the gridded CRU TS precipitation dataset with the point RGR over the TRHR during 1961-2014. The temporal trends and spatial distributions of precipitation were analyzed based on these two datasets, respectively, and the relationship of precipitation derived from the gridded dataset with elevation was analyzed. Moreover, the obtained results were comprehensively compared and discussed. The significances of this study can be summarized as follows.

First, for both datasets, the annual precipitation presented a significant increasing trend (p<0.1) in the TRHR during 1961-2014, and the spatial distribution of the MAP over this region had the southeast-to-northwest decreasing trend. Second, for the CRU TS dataset, the annual precipitation recorded at all the grids presented the increasing trends, and a low-to-high increasing trend in the MAP was found for grids with the elevations below 3,800 m but an inverse correlation for grids with the elevations above 3,800 m; moreover, statistical equations which integrated longitude, latitude and elevation were established to estimate the MAP derived from the gridded CRU TS dataset over this region. Third, through comparing the results derived from the two datasets, we found that the annual precipitation values derived from the CRU TS dataset were much smaller than those derived from the RGR data, although the two series had the similar variation characteristics during 1961-2014. Finally, the MAP values derived from the gridded CRU TS dataset could be well estimated by using the equations derived from the RGR data.

This study contributed to provide a scientific basis for the utilization of the gridded precipitation dataset in high-elevation mountainous regions such as the TRHR, which will be valuable for handling the water-related issues in the future, e.g., integrated water resources management and ecological environment assessment.

Acknowledgements

This study was supported by the Hong Kong Scholars Program project (XJ2014059) and the Non-profit Fund Program of the Ministry of Water Resources of China (201501028). We are also grateful to the associate editor and the two anonymous reviewers who offered the insightful comments leading to improvement of this paper.

References

ASTER GDEM Validation Team. 2009. ASTER global DEM validation summary report. METI & NASA.

ASTER GDEM Validation Team. 2011. ASTER global DEM version 2 – summary of validation results. METI & NASA.

Becker, A., Finger, P., Meyer-Christoffer, A., Rudolf, B., Schamm, K., Schneider, U., Ziese, M., 2013. A description of the global land-surface precipitation data products of the global precipitation climatology centre with sample applications including centennial (trend) analysis from 1901-present. *Earth System Science Data*, 5, 71-99.

Belo-Pereira, M., Dutra, E., Viterbo, P., 2011. Evaluation of global precipitation data sets over the Iberian Peninsula. *Journal of Geographical Research*, 116, D20101.

Boos, W.R., Kuang, Z.M., 2010. Dominant control of the South Asian Monsoon by orographic insulation versus plateau heating. *Nature*, 463, 218-222.

Bosilovich, M.G., Chen, J., Robertson, F.R., Adler, R.F., 2008. Evaluation of global precipitation in reanalyses. *Journal of Applied Meteorology & Climatology*, 47, 2279-2299.

Brassel, K.E., Reif, D., 1979. A procedure to generate Thiessen polygons. *Geographical Analysis*, 11, 289-303.

Cao, L.G., Pan, S.M., 2014. Changes in precipitation extremes over the "Three-River Headwaters" region, hinterland of the Tibetan Plateau, during 1960-2012. *Quaternary International*, 321, 105-115.

China Meteorological Administration, 2016. Daily meteorological observation data sets of China. http://data.cma.gov.cn/data/detail/dataCode/SURF_CLI_CHN_MUL_DAY_V3.0.html.

Chen, D.L., Tian, Y.D., Yao, T.D, Ou, T.H., 2016. Satellite measurements reveal strong anisotropy in spatial coherence of climate variations over the Tibet Plateau. *Scientific Reports*, 6, 30304.

Chen, Y.R., Chu, P.S., 2014. Trends in precipitation extremes and return levels in the Hawaiian Islands under a changing climate. *International Journal of Climatology*, 34(15), 3913-3925.

Chu, H.J., 2012. Assessing the relationships between elevation and extreme precipitation with various durations in southern Taiwan using spatial regression models. *Hydrological Processes*, 26(21), 3174-3181.

Curio, J., Scherer, D., 2016. Seasonality and spatial variability of dynamic precipitation controls on the Tibetan Plateau. *Earth System Dynamics*, 7, 767-782.

Dirks, K.N., Hay, J.E., Stow, C.D., Harris, D., 1998. High-resolution studies of rainfall on Norfolk Island: Part II: Interpolation of rainfall data. *Journal of Hydrology*, 208(3-4), 187-193.

Fan, J.W., Shao, Q.Q., Liu, J.Y., Wang, J.B., Harris, W., Chen, Z.Q., Zhong, H.P., Xu, X.L., Liu, R.G., 2010. Assessment of effects of climate change and grazing activity on grassland yield in the Three Rivers Headwaters Region of Qinghai-Tibet Plateau, China. *Environmental Monitoring and Assessment*, 170(1-4), 571-584.

Goovaerts, P., 2000. Geostatistical approaches for incorporating elevation into the spatial interpolation of rainfall. *Journal of Hydrology*, 228, 113-129.

Harris, I.C., Jones, P.D., Osborn, T.J., Lister, D.H., 2014. Updated high-resolution grids of monthly climatic observations - the CRU TS 3.10 Dataset. *International Journal of Climatology*, 34, 623-642.

Harris, I.C., Jones, P.D., 2015. CRU TS3.23: Climatic Research Unit (CRU) Time-Series (TS) Version 3.23 of High Resolution Gridded Data of Month-by-month Variation in Climate

(Jan. 1901 - Dec. 2014). *Centre for Environmental Data Analysis*, 09 November 2015. doi: 10.5285/4c7fdfa6-f176-4c58-acee-683d5e9d2ed5.

Huang K., Zhang, Y.J., Zhu, J.T., Liu, Y.J., Zu, J.X., Zhang, J., 2016. The influences of climate change and human activities on vegetation dynamics in the Qinghai-Tibet Plateau. *Remote Sensing*, 8, 876.

Immerzeel, W.W., van Beek, L.P.H., Bierkens, M.F.P., 2010. Climate change will affect the Asian water towers. *Science*, 328, 1382-1385.

Intergovernmental Panel on Climate Change (IPCC), 2013. Climate Change 2013: The Physical Science Basis. *Contribution of Working Group I to the Fifth Assessment Report of the IPCC*, Cambridge University Press, Cambridge, United Kingdom and New York, USA.

Jones, J.R., Schwartz, J.S., Ellis, K.N., Hathaway, J.M., Jawdy, C.M., 2015. Temporal variability of precipitation in the Upper Tennessee Valley. *Journal of Hydrology: Regional Studies*, 3, 125-138.

Jones, P.D., Harpham, C., Harris, I.C., et al., 2016. Long-term trends in precipitation and temperature across the Caribbean. *International Journal of Climatology*, 36, 3314-3333.

Kendall, M.G., 1975. *Rank Correlation Measures*. London: Charles Griffin.

Khalili, A., Rahimi, J., 2014. High-resolution spatiotemporal distribution of precipitation in Iran: a comparative study with three global-precipitation datasets. *Theoretical and Applied Climatology*, 118, 211-221.

Kistler, R., Kalnay, E., Collins, W., Saha, S., White, G., Woollen, J., Chelliah, M., Ebisuzaki,W., Kanamitsu, M., Kousky, V., Van den Dool, H., Jenne, R., Fiorino, M., 2001. The NCEP-NCAR 50-year reanalysis: monthly means CD-ROM and documentation. *Bulletin of the American Meteorological Society*, 82, 247-267.

Li, X.H., Zhang, Q., Xu, C.Y., 2012. Suitability of the TRMM satellite rainfalls in driving a distributed hydrological model for water balance computations in Xinjiang catchment, Poyang lake basin. *Journal of Hydrology*, 426, 28-38.

Liang, L.Q., Li, L.J., Liu, C.M., Cuo, L., 2013. Climate change in the Tibetan Plateau Three Rivers Source Region: 1960-2009. *International Journal of Climatology*, 33, 2900-2916.

Lin, R., Zhou, T., Qian, Y., 2014. Evaluation of global monsoon precipitation changes based on five reanalysis datasets. *Journal of Climate*, 27, 1271-1289.

Liu, Q., Yang, Z.F., Cui, B.S., 2008. Spatial and temporal variability of annual precipitation during 1961-2006 in Yellow River Basin, China. *Journal of Hydrology*, 361, 330-338.

Ma, L., Zhang, T., Frauenfeld, O.W., Ye, B., Yang, D., Qin, D., 2009. Evaluation of precipitation from the ERA-40, NCEP-1, and NCEP-2 reanalyses and CMAP-1, CMAP-2, and GPCP-2 with ground-based measurements in China. *Journal of Geophysical Research: Atmospheres*, 114, D09105.

Mann, H.B., 1945. Non-parametric tests against trend. *Econometrica*, 13, 245-259.

Mishra, A.K., Gairola, R.M., Varma, A.K., et al., 2011. Improved rainfall estimation over the Indian region using satellite infrared technique. *Advances in Space Research*, 48(1), 49-55.

Mito, Y., Ismail, M.A.M., Yamamoto, T., 2011. Multidimensional scaling and inverse distance weighting transform for image processing of hydrogeological structure in rock mass. *Journal of Hydrology*, 411(1-2), 25-36.

Mu, X.M., Zhang, L., McVicar, T.R., Chille, B., Gau, P., 2007. Analysis of the impact of conservation measures on stream flow regime in catchments of the Loess Plateau, China. *Hydrological Processes*, 21, 2124-2134.

Nash, J.E., Sutcliffe, J.V., 1970. River flow forecasting through conceptual models part 1 - A discussion of principles. *Journal of Hydrology*, 10(3), 282-290.

Nezlin, N.P., Stein, E.D., 2005. Spatial and temporal patterns of remotely-sensed and field-measured rainfall in southern California. *Remote Sensing of Environment*, 96(2), 228-245.

Pettitt, A.N., 1979. A non-parametric approach to the change-point problem. *Applied Statistics*, 28(2), 126-135.

Schermerhorn, V.P., 1967. Relations between topography and annual precipitation in western Oregon and Washington. *Water Resources Research*, 3(3), 707-711.

Schneider, U., Becker, A., Finger, P., Meyer-Christoffer, A., Ziese, M., Rudolf, B., 2014. GPCC's new land surface precipitation climatology based on quality-controlled in situ data and its role in quantifying the global water cycle. *Theoretical and Applied Climatology*, 115, 15-40.

Sen, P.K., 1968. Estimates of the regression coefficient based on Kendall's tau. *Journal of the American Statistical Association*, 63, 1379-1389.

Shao, Q.Q., Zhao, Z.P., Liu, J.Y., Fan, J.W., 2010. The characteristics of land cover and macroscopical ecology changes in the source region of three rivers on Qinghai-Tibet Plateau during last 30 years. *Geographical Research*, 29(8), 1139-1451. [In Chinese]

Shi, H.Y., 2013. Computation of spatially distributed rainfall by merging raingauge measurements, satellite observations and topographic information: A case study of the 21 July 2012 rainstorm in Beijing, China. *Proceedings of the 35th IAHR World Congress*, vols I and II, 530-542.

Shi, H.Y., Fu, X.D., Chen, J., Wang, G.Q., Li, T.J., 2014. Spatial distribution of monthly potential evaporation over mountainous regions: case of the Lhasa River basin, China. *Hydrological Sciences Journal*, 59(10), 1856-1871.

Shi, H.Y., Li, T.J., Wei, J.H., Fu, W., Wang, G.Q., 2016a. Spatial and temporal characteristics of precipitation over the Three-River Headwaters region during 1961-2014. *Journal of Hydrology: Regional Studies*, 6, 52-65.

Shi, H.Y., Li, T.J., Wang, K., Zhang, A., Wang, G.Q., Fu, X.D., 2016b. Physically based simulation of the streamflow decrease caused by sediment-trapping dams in the middle Yellow River. *Hydrological Processes*, 30(5), 783-794.

Shi, H.Y., Li, T.J., Wang, G.Q., 2017. Temporal and spatial variations of potential evaporation and the driving mechanism over Tibet during 1961-2001. *Hydrological Sciences Journal*, in press.

Shi, H.Y., Wang, G.Q., 2015. Impacts of climate change and hydraulic structures on runoff and sediment discharge in the middle Yellow River. *Hydrological Processes*, 29(14), 3236-3246.

Silva, V.B.S., Kousky, V.E., Higgins, R.W., 2011. Daily precipitation statistics for South America: an intercomparison between NCEP reanalyses and observations. *Journal of Hydrometeorology*, 12, 101-117.

Sohn, S.-J., Tam, C.-Y., Ashok, K., Ahn, J.-B., 2012. Quantifying the reliability of precipitation datasets for monitoring large-scale East Asian precipitation variations. *International Journal of Climatology*, 32, 1520-1526.

Thiel, H., 1950. A rank-invariant method of linear and polynomial regression analysis, III. *Proceedings of Koninalijke Nederlandse Akademie van Weinenschatpen*, 53, 1397-1412.

Thiessen, A.J., Alter, J.C., 1911. Precipitation Averages for Large Areas. *Monthly Weather Review*, 39, 1082-1984.

Tong, L.G., Xu, X.L., Fu, Y., Li, S., 2014. Wetland Changes and Their Responses to Climate Change in the “Three-River Headwaters” Region of China since the 1990s. *Energies*, 7, 2515-2534.

von Storch, H., Navarra, A., 1995. *Analysis of Climate Variability: Applications of Statistical Techniques*. Berlin: Springer-Verlag.

Woldemeskel, F.M., Sivakumar, B., Sharma, A., 2013. Merging gauge and satellite rainfall with specification of associated uncertainty across Australia. *Journal of Hydrology*, 499, 167-176.

Yi, X.S., Li, G.S., Yin, Y.Y., 2013. Spatio-temporal variation of precipitation in the Three-River Headwater Region from 1961 to 2010. *Journal of Geographical Sciences*, 23(3), 447-464.

Yu, W.S., Ma, Y.M., Sun, W.Z., Wang, Y., 2009. Climatic significance of δ^{18}O records from precipitation on the western Tibetan Plateau. *Chinese Science Bulletin*, 54(16), 2732-2741.

Zarch, M.A.A., Sivakumar, B., Sharma, A., 2015. Droughts in a warming climate: A global assessment of Standardized precipitation index (SPI) and Reconnaissance drought index (RDI). *Journal of Hydrology*, 526, 183-195.

Zhang, A.J., Zheng, C.M., Wang, S., Yao, Y.Y., 2015. Analysis of streamflow variations in the Heihe River Basin, northwest China: Trends, abrupt changes, driving factors and ecological influences. *Journal of Hydrology: Regional Studies*, 3, 106-124.

Zhang, T., Zhan, J.Y., Huang, J., Yu, R., Shi, C.C., 2013. An Agent-Based Reasoning of Impacts of Regional Climate Changes on Land Use Changes in the Three-River Headwaters Region of China. *Advances in Meteorology*, 248194.

Zhao, T., Fu, C., 2006. Comparison of products from ERA-40, NCEP-2, and CRU with station data for summer precipitation over China. *Advances in Atmospheric Sciences*, 23, 593-604.

Zhu, X.F., Zhang, M.J., Wang, S.J., Qiang, F., Zeng, T., Ren, Z.G., Dong, L., 2015. Comparison of monthly precipitation derived from high-resolution gridded datasets in arid Xinjiang, central Asia. *Quaternary International*, 358, 160-170.

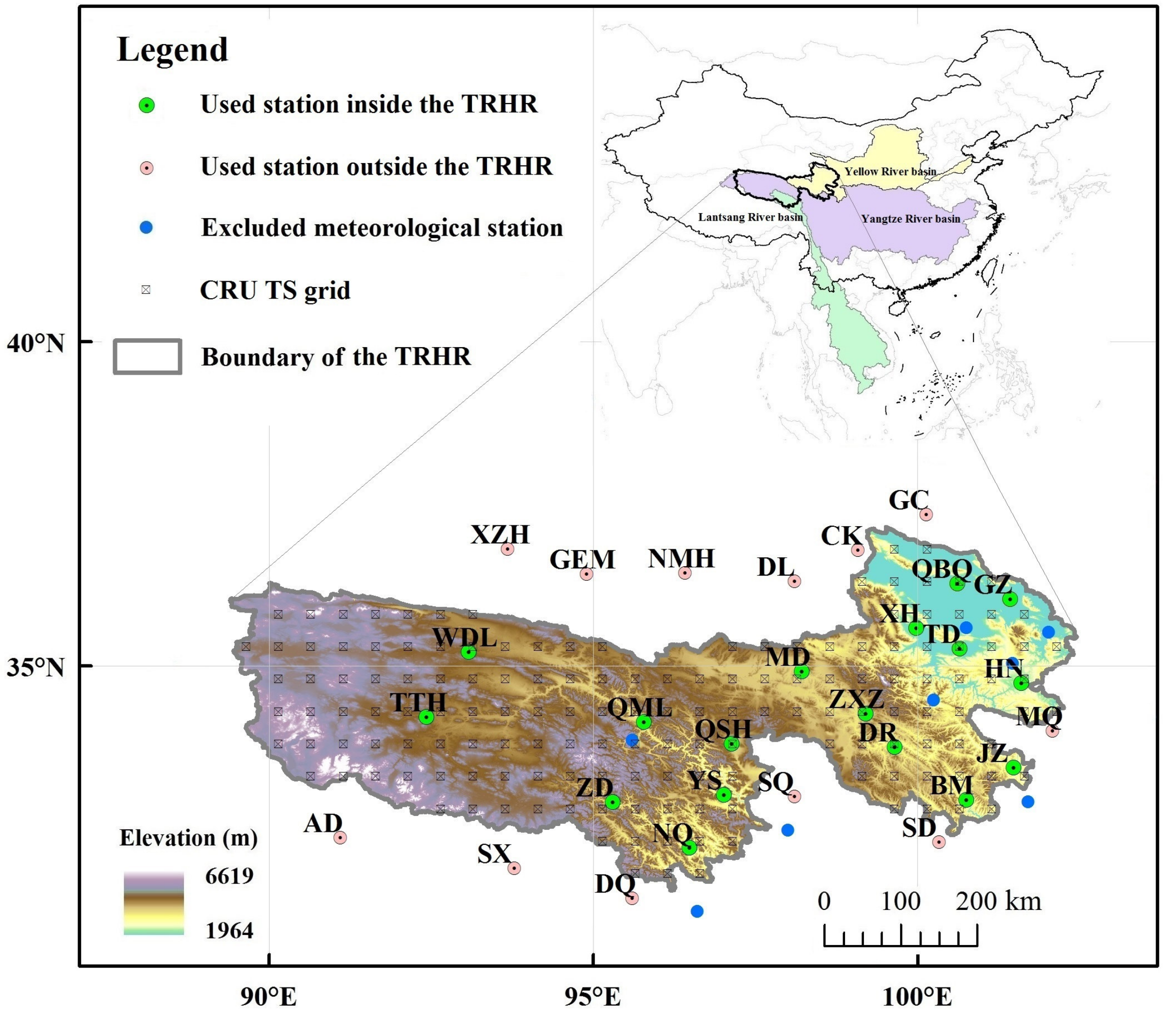

Fig. 1 The distribution of the CRU TS grids with the horizontal resolution of 0.5×0.5 degree and the locations of meteorological stations over the TRHR.

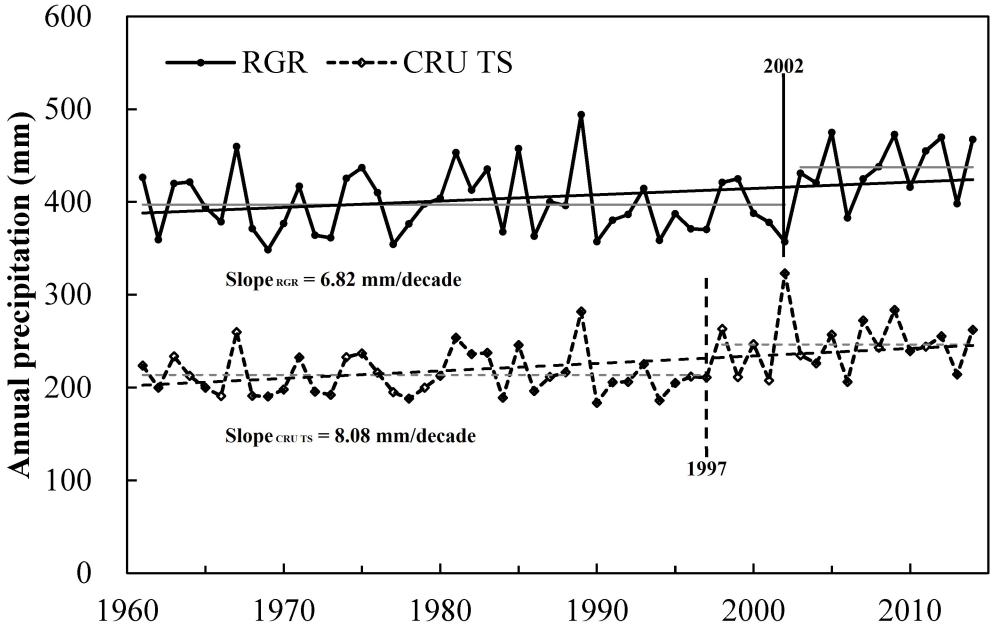

Fig. 2 The annual precipitation series derived from the CRU TS dataset and the RGR data over the TRHR during 1961-2014. Note: The horizontal lines in grey show the mean annual precipitation of the subsequences for the CRU TS dataset (dash) and the RGR data (solid).

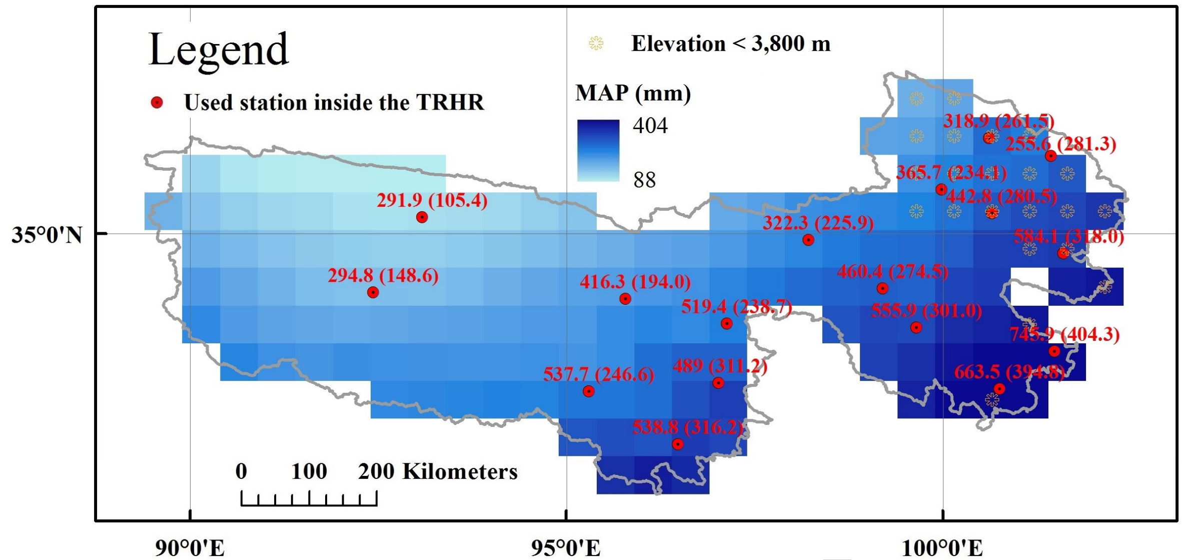

Fig. 3 Spatial distribution of the mean annual precipitation in each grid or station over the TRHR during 1961-2014. Note: The values out of parentheses are derived from the RGR data, and the values in parentheses are derived from the CRU TS data in the corresponding grid.

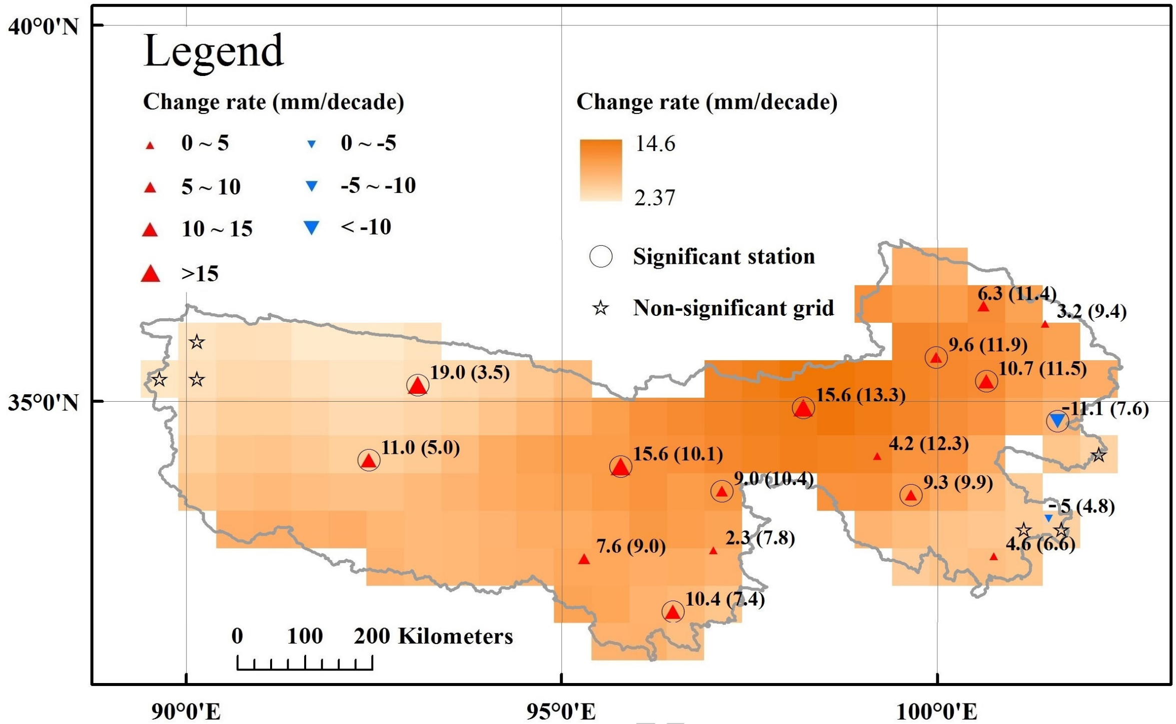

Fig. 4 Spatial distribution of the change rate of the annual precipitation in each grid or station over the TRHR during 1961-2014. Note: The values out of parentheses are derived from the RGR data, and the values in parentheses are derived from the CRU TS data in the corresponding grid.

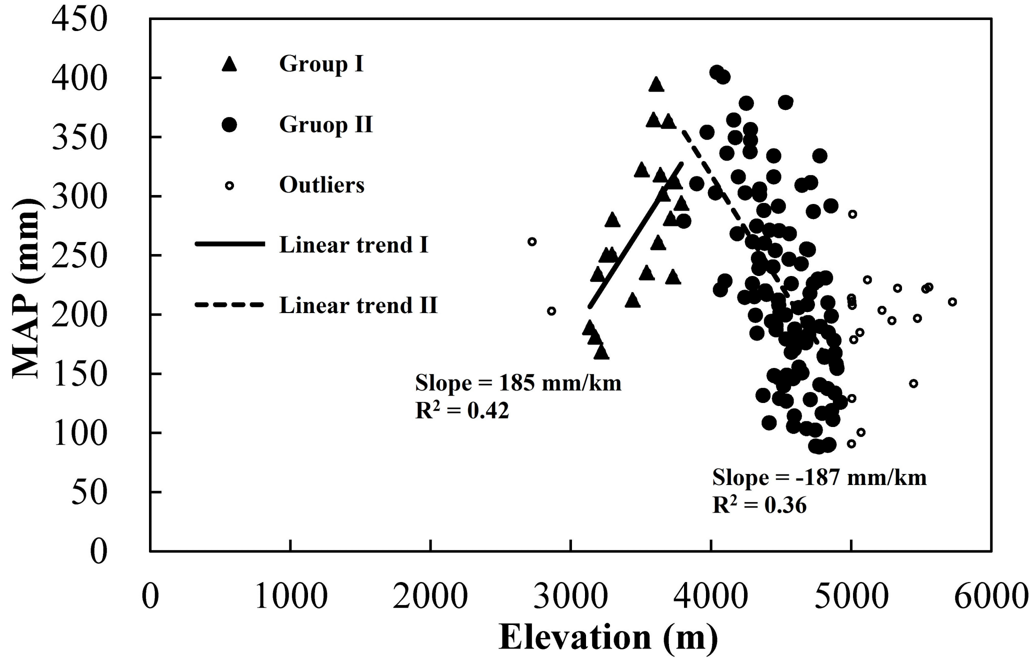

Fig. 5 Relationship between the mean annual precipitation and elevation in each grid over the TRHR during 1961-2014.

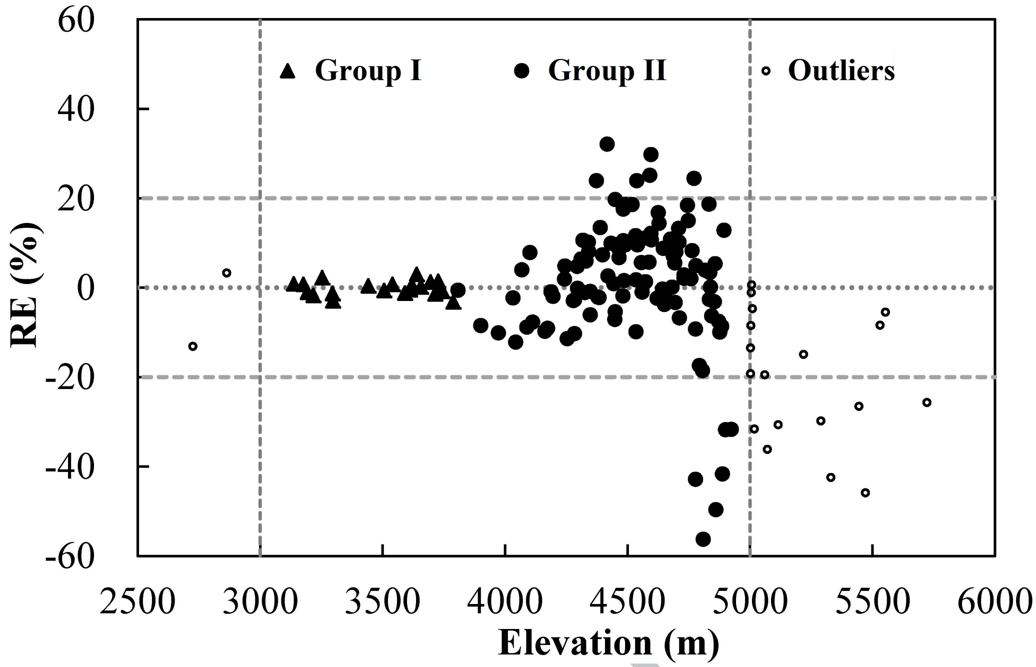

Fig. 6 Comparison of the MAP values estimated by equation (5) and the observations in each grid of the CRU TS dataset.

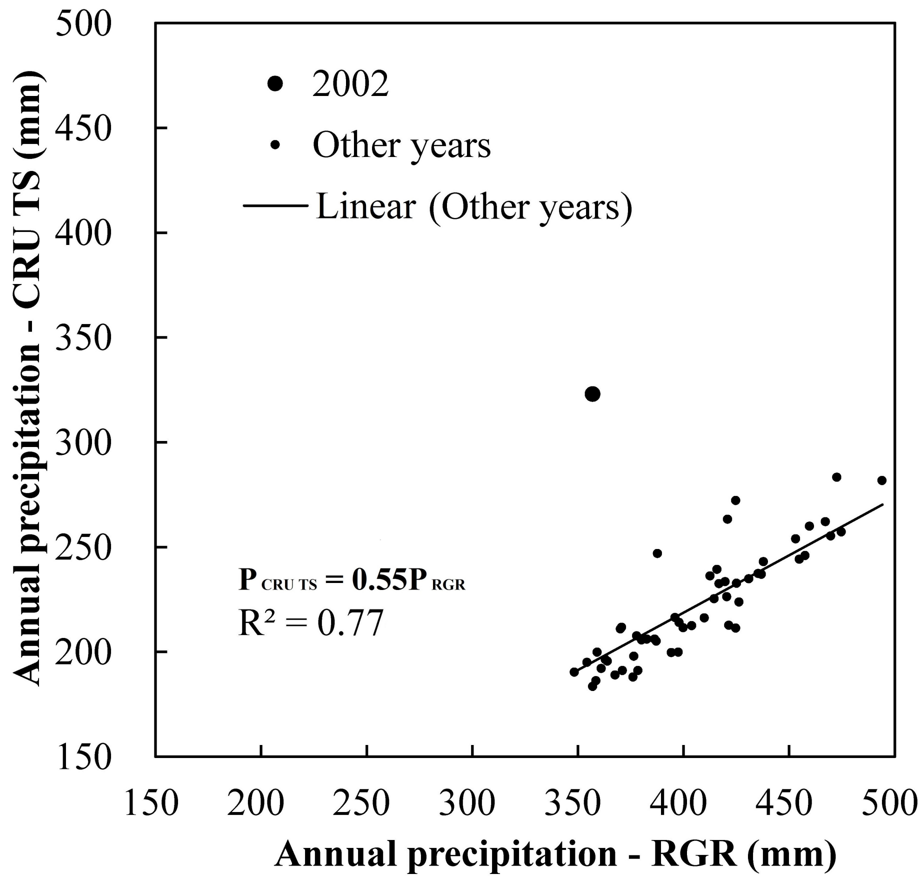

Fig. 7 The relationship between the annual precipitation series derived from the CRU TS dataset and the RGR data over the TRHR during 1961-2014.

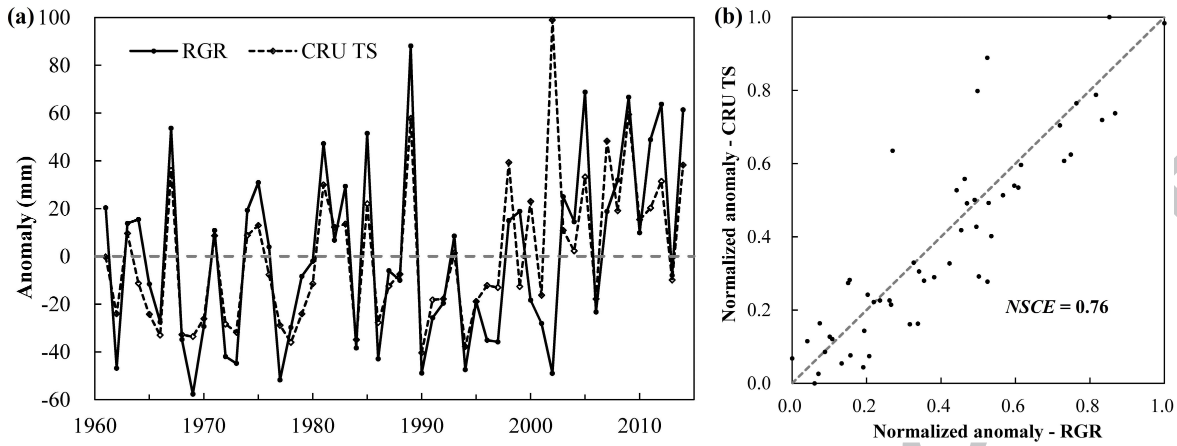

Fig. 8 (a) The anomalies of the annual precipitation series derived from the CRU TS dataset and the RGR data over the TRHR during 1961-2014; (b) The relationship between the normalized anomalies derived from the two datasets (except 2002).

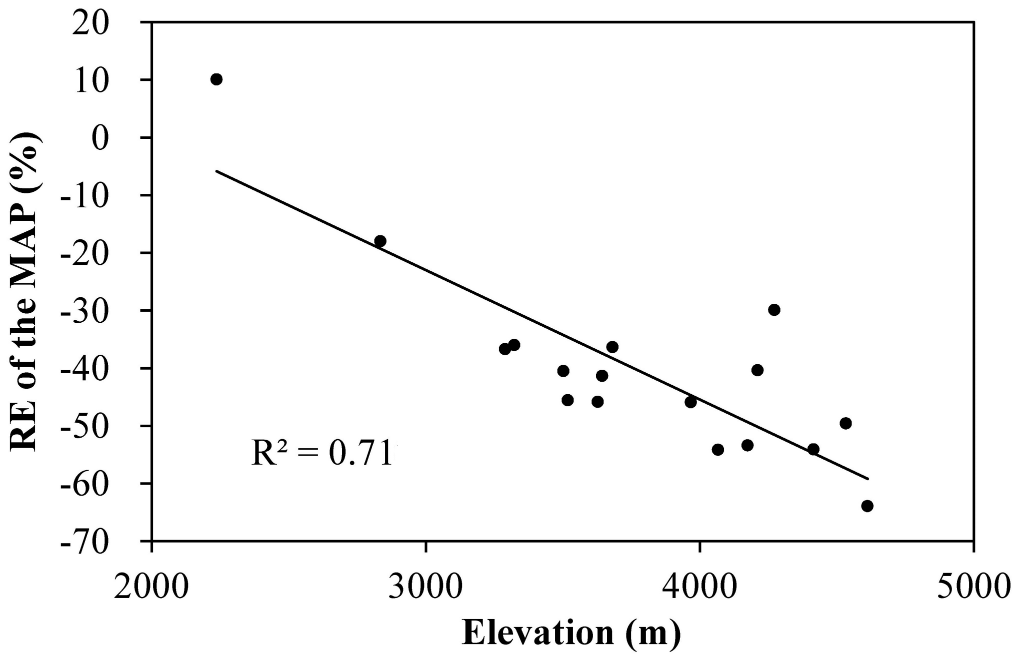

Fig. 9 Relationship between the RE values of the MAP and elevation for each station located inside the TRHR and the corresponding grid.

Table 1. General information of the meteorological stations over the TRHR

Station name	Abbreviation	Longitude (°E)	Latitude (°N)	Elevation (m)	Years with observed data
Qiaboqia	**QBQ**	**100.62**	**36.27**	**2835**	**1953-2014**
Guizhou	**GZ**	**101.43**	**36.03**	**2237**	**1956-2014**
Wudaoliang	**WDL**	**93.08**	**35.22**	**4612**	**1956-2014**
Xinghai	**XH**	**99.98**	**35.58**	**3323**	**1960-2014**
Tongde	**TD**	**100.65**	**35.27**	**3289**	**1954-1998**
Tuotuohe	**TTH**	**92.43**	**34.22**	**4533**	**1956-2014**
Zaduo	**ZD**	**95.30**	**32.90**	**4066**	**1956-2014**
Qumalai	**QML**	**95.78**	**34.13**	**4175**	**1956-2014**
Yushu	**YS**	**97.02**	**33.02**	**3681**	**1951-2014**
Maduo	**MD**	**98.22**	**34.92**	**4272**	**1953-2014**
Qingshuihe	**QSH**	**97.13**	**33.80**	**4415**	**1956-2014**
Zhongxinzhan	**ZXZ**	**99.20**	**34.27**	**4211**	**1959-1997**
Dari	**DR**	**99.65**	**33.75**	**3968**	**1956-2014**
Henan	**HN**	**101.60**	**34.73**	**3519**	**1959-2014**
Jiuzhi	**JZ**	**101.48**	**33.43**	**3629**	**1958-2014**
Nangqian	**NQ**	**96.48**	**32.20**	**3644**	**1956-2014**
Banma	**BM**	**100.75**	**32.93**	**3503**	**1960-2014**
Seda	SD	100.33	32.28	3929	1961-2014
Suoxian	SX	93.78	31.88	4023	1956-2014
Dingqing	DQ	95.60	31.42	3873	1954-2014
Maqu	MQ	102.08	34.00	3471	1967-2014
Shiqu	SQ	98.10	32.98	4086	1960-2014
Anduo	AD	91.10	32.35	4800	1965-2014
Xiaozhaohuo	XZH	93.68	36.80	2767	1960-2014
Gangcha	GC	100.13	37.33	3321	1957-2014
Geermu	GEM	94.9	36.42	2807.6	1955-2014
Nuomuhong	NMH	96.42	36.43	2790	1956-2014
Dulan	DL	98.10	36.30	3191	1954-2014
Chaka	CK	99.08	36.78	3088	1955-2000
Guinan	*/*	*100.75*	*35.58*	*3150*	*1999-2014*
Zeku	*/*	*101.47*	*35.03*	*3663*	*1957-1990*
Tongren	*/*	*102.02*	*35.52*	*2491*	*1991-2014*
Zhiduo	*/*	*95.6*	*33.85*	*4179*	*1961-1990*
Guoluo	*/*	*100.25*	*34.47*	*3719*	*1991-2014*
Leiwuqi	*/*	*96.60*	*31.22*	*3810*	*1991-2014*
Shiquluoxu	*/*	*98.00*	*32.47*	*3399*	*1960-1981*
Aba	*/*	*101.7*	*32.90*	*3275*	*1954-1990*

Note: (1) Stations in bold format are located inside the TRHR. (2) Stations in italic format are excluded in this study.

Table 2. Results of trend and change point tests for the annual precipitation series derived from the CRU TS dataset and the RGR data over the TRHR during 1961-2014

Data	Change point	Period	Mean value (mm)	Slope (mm/decade)
CRU TS	1997	1961-2014	224.0	8.08
		1961-1997	213.7	0.39
		1998-2014	246.5	2.53
RGR	2002	1961-2014	406.0	6.82
		1961-2002	397.0	-2.45
		2003-2014	437.5	18.6

Table 3. Results of the RE analysis for the annual precipitation series derived from the CRU TS dataset and the RGR data over the TRHR during 1961-2014

Maximum		Minimum		Minimum (except 2002)		Mean (except 2002)
Value	Year	Value	Year	Value	Year	
-50%	1999	-9%	2002	-36%	2007	-45%

Table 4. Comparison of the MAP values and change rates for each station located inside the TRHR and the corresponding grid

Station	Elevation (m)	MAP (mm)			Change rate (mm/decade)		
		RGR	CRU TS	RE (%)	RGR	CRU TS	RE (%)
QBQ	2835	318.9	261.5	-18	6.33	11.40	80
GZ	2237.1	255.6	281.3	10	3.21	9.36	192
WDL	4612.2	291.9	105.4	-64	19.00	3.51	-82
XH	3323.2	365.7	234.1	-36	9.62	11.91	24
TD	3289.4	442.8	280.5	-37	10.67	11.46	7.5
TTH	4533.1	294.8	148.6	-50	11.00	5.00	-55
ZD	4066.4	537.7	246.6	-54	7.56	8.97	19
QML	4175	416.3	194.0	-53	15.63	10.11	-35
YS	3681.2	489.0	311.2	-36	2.25	7.79	246
MD	4272.3	322.3	225.9	-30	15.57	13.28	-15
QSH	4415.4	519.4	238.7	-54	9.04	10.44	15
ZXZ	4211.1	460.4	274.5	-40	4.21	12.31	192
DR	3967.5	555.9	301.0	-46	9.33	9.93	6.4
HN	3519	584.1	318.0	-46	-11.06	7.64	-169
JZ	3628.5	745.9	404.3	-46	-5.00	4.82	-196
NQ	3643.7	538.8	316.2	-41	10.43	7.35	-30
BM	3503	663.5	394.8	-40	4.56	6.57	44

Table 5. Comparison of the MAP values estimated by equations (5) and (7) for each grid corresponding to the station located inside the TRHR

Station	MAP (mm)	Equation (5)		Equation (7)	
		MAP (mm)	RE (%)	MAP (mm)	RE (%)
QBQ	261.5	227.3	-13.1	157.2	-39.9
GZ	281.3	277.4	-1.4	303.4	7.8
WDL	105.4	131.8	25.1	136.2	29.3
XH	234.1	231.6	-1.1	211.7	-9.6
TD	280.5	272.1	-3.0	251.8	-10.2
TTH	148.6	162.8	9.5	180.3	21.3
ZD	246.6	260.3	5.6	280.5	13.8
QML	194.0	213.1	9.8	214.4	10.5
YS	311.2	289.9	-6.8	300.1	-3.6
MD	225.9	236.6	4.7	219.2	-3.0
QSH	238.7	257.9	8.1	256.4	7.4
ZXZ	274.5	271.4	-1.1	254.0	-7.5
DR	301.0	298.2	-0.9	283.6	-5.8
HN	318.0	327.4	3.0	329.3	3.6
JZ	404.3	354.8	-12.3	334.0	-17.4
NQ	316.2	309.7	-2.0	326.3	3.2
BM	394.8	393.1	-0.4	369.6	-6.4

Research Highlights

1. Detection of spatial-temporal variation of precipitation
2. Investigation of the correlation of precipitation with elevation
3. Establishment of statistical equations based on longitude, latitude and elevation
4. Evaluation of the gridded CRU TS dataset with the point raingauge records

ACCEPTED MANUSCRIPT